Response and Hub Loads Sensitivity Analysis of a Helicopter Rotor

Joon W. Lim* and Inderjit Chopra†
University of Maryland, College Park, Maryland

A sensitivity study of blade response and oscillatory hub loads in forward flight for a hingeless rotor with respect to structural design variables is examined. Structural design variables include nonstructural mass distribution (spanwise and chordwise), chordwise offset of center of gravity, and blade bending stiffnesses (flap, lag, and torsion). The blade is discretized into a number of beam elements, and response equations are transformed into the normal mode space. The nonlinear, periodic, steady response of the blade is calculated using a finite element in time approach. Then, the vehicle trim and blade steady response are calculated iteratively as one coupled solution using a modified Newton method. The formulation for the derivatives of blade response and hub loads is implemented, using a direct analytical approach (chain rule differentiation), and forms an integral part of the basic response analysis. For calculation of the sensitivity derivatives, a 96% reduction of CPU time is achieved by using the direct analytical approach, compared with the finite-difference approach.

Introduction

STRUCTURAL optimization with aeroelastic constraints has received considerable attention in the fixed-wing field.[1] With an enhanced understanding of the dynamics of rotary-wing systems, it is now becoming feasible to apply structural optimization to the rotary-wing field. The potential of structural optimization is further expanded with the application of composites in blade construction, which permits great flexibility in tailoring structural characteristics. Also, the techniques of modern structural optimization have become more refined, the data processing capability of modern computers has grown substantially, and it is becoming attractive to implement aeroelastic optimization to complex rotor systems.

There have been few attempts to explore aeroelastic optimization of a rotor blade for vibration reduction. Blackwell[2] made a sensitivity study of several rotor design parameters on oscillatory hub loads of a four-bladed articulated rotor and pointed out the potential of a vibration reduction of a helicopter through an optimized blade design. Taylor[3] considered the minimization of a modal shaping parameter. The response of a particular mode to the aerodynamic excitation was minimized by adjusting the mode shape. Friedmann and Shanthakumaran[4] applied a modern structural optimization procedure using a sequential unconstrained minimization technique (SUMT[5]) to reduce oscillatory hub loads for a four-bladed hingeless rotor by redistributing the mass and stiffness properties on the rotor blades. They imposed constraints on frequency placements and aeroelastic stability in hover. Results showed a 15-40% reduction in oscillatory vertical hub shear for a soft-inplane hingeless rotor. Peters et al.[6] have applied an optimization technique (CONMIN[7]) to place the rotating natural frequencies by distributions of mass and stiffness properties of rotor blades. Then, the optimum design was pursued for a minimum blade weight with a constraint on its flap inertia. However, comprehensive aeroelastic analysis was not considered, and stability constraints were not imposed in the optimization process. Davis and Weller[8] applied a constrained optimization code called an Automated Design Synthesis (ADS[9]) to solve four different rotor problems: maximizing bearingless rotor inplane damping, placing blade natural frequencies, minimizing hub vertical shear, and minimizing rotor modal vibration indices. However, aeroelastic stability constraints were not considered in the optimization process. Yen[10] showed that a significant reduction in oscillatory hub loads could be achieved by structural optimization of the rotor blades. In this paper, a correlation of wind tunnel data with theoretical hub loads was attempted for an optimized rotor. All of these papers showed the potential of structural optimization to the rotary-wing field.

Aeroelastic optimization of a system essentially consists of the determinations of the optimum values of design variables that minimize the objective function and satisfy certain aeroelastic and geometric constraints. One of the key elements of an optimization analysis is the sensitivity analysis. The sensitivity analysis helps to assess the influence of variations of the design variables on response and analytical modeling, and guide the selection of the important design variables. Also, for the aeroelastic optimization algorithms, one needs the derivatives of structural response quantities, such as hub loads, structural bending and blade response, and the derivatives of aeroelastic constraints, such as blade eignevalues with respect to the design variables. In fact, the sensitivity analysis constitutes a major part of the total optimization calculation. Rotor dynamics is complex and involves nonlinear inertia, elastic, and aerodynamic loads. Therefore, it is important to carry out the design sensitivity analysis as efficiently as possible for the complex rotor optimization problems. For analytical calculations of the sensitivity derivatives, Adelman and Haftka[11] have given a general survey paper on the sensivity analysis of discrete structural systems. The survey discusses various methods for calculating the sensitivity derivatives of static displacements and stresses, eigenvalues and eigenvectors, transient structural response, and the derivatives of optimum structural designs with respect to the design variables. The need for sensitivity analysis in complex structural optimization problems has been stressed.

Most of the existing rotor optimization studies use finite-difference approaches to calculate the sensitivity derivatives,

Presented as Paper 87-0923 at the AIAA Dynamics Specialists Conference, Monterey, CA, April 9-10, 1987; received Sept. 26, 1988; revision received March 20, 1989.

*Research Associate, Department of Aerospace Engineering; currently Engineering Specialist, Bell Helicopter Textron, Ft. Worth, Texas. Member AIAA.

†Professor, Department of Aerospace Engineering. Associate Fellow AIAA.

and, therefore, involve a large computation time to obtain an optimum solution. Because of the large computation time involved, these studies are restrictive in terms of objective functions, dynamic constraints, and the number of design variables. The present paper focuses on this important issue. A direct analytical approach coupled with the finite-element method in time is developed for calculation of the sensitivity derivatives of response and hub loads of a helicopter rotor in forward flight. With this approach, the formulation of the sensitivity derivatives forms an integral part of the basic response analysis and these derivatives are, therefore, obtained at a fraction of computation time as compared to the frequently adopted finite-difference approaches.

For an effective aeroelastic sensitivity analysis, one needs a reliable rotor dynamic analysis to determine steady response of a rotor system in forward flight. Over the years, there have been several contributions to developing a reliable procedure for the rotor dynamic analysis (see, for example, Refs. 12 and 13). The rotor dynamic analysis used in the present study was developed at the University of Maryland and is based on the finite-element method in space and time.[14,15] This analysis consists of coupled vehicle trim and rotor steady response. The vehicle trim solution determines the control settings and vehicle attitude for the prescribed flight condition. The steady response involves the determination of time-dependent blade deflections at different azimuth for one complete cycle, using a finite-element method in time. The vehicle trim and blade steady response are calculated iteratively as one coupled solution, using a modified Newton method.

Using a direct analytical approach, the sensitivity derivatives of blade steady response and oscillatory hub forces and moments are obtained. To justify this approach, the numerical results are compared with the finite-difference approach. Through a parametric study of several design parameters, the sensitivity of oscillatory hub loads is also examined. Results are presented for a typical four-bladed soft-inplane hingless rotor.

Analysis

The rotor dynamics analysis used in the present study is based on a finite-element method in space and time.[14,15] For the analysis, each blade is assumed to be an elastic beam undergoing flap bending, lag bending, elastic twist, and axial deflections. The blade is discretized into a number of beam elements. Each beam element consists of 15 degrees of freedom. Between elements, there is a continuity of displacement and slope for lag and flap bending deflections, and a continuity of displacement for elastic twist and axial deflections. The analysis is developed for a nonuniform blade having pretwist, precone, and chordwise offsets of blade center of gravity, aerodynamic center, and tensile axis from the elastic axis.

Aerodynamic loads are based on a quasisteady strip theory approximation. The noncirculatory loads based on unsteady thin airfoil theory are also included. For the steady induced inflow distribution on the rotor disk, a linear inflow model due to Johnson[16] is used.

Coupled trim analysis in forward flight[15,17] determines vehicle trim (propulsive), blade steady response, and hub loads. To start the calculation process, first the uncoupled vehicle trim solution is calculated from the overall nonlinear vehicle equilibrium equations for a rigid flapping blade model. For a specified advance ratio μ and weight coefficient c_W, the trim solution gives pitch-control settings $\theta_{0.75}, \theta_{1c}, \theta_{1s}$ and vehicle attitude α_s, ϕ_s. This uncoupled trim solution is used as an initial guess for the iteration process of the complete trim solution.

The blade steady response solution involves the determination of time-dependent blade deflections at different azimuth locations. To reduce computation time, the finite-element equations are transformed to the normal mode domain, using the coupled natural vibration modes of the blade. These nonlinear periodic equations are then solved, using the finite-element method in time. The hub loads are obtained using a force summation method. For this, motion-induced aerodynamic and inertial loads are integrated along the blade span to obtain blade loads at the root, and then summed over all the blades to obtain rotor hub loads.

For the coupled trim analysis, the vehicle trim and rotor response equations are calculated iteratively as one coupled solution, using a modified Newton method. During the iteration process, pitch-control settings and vehicle change, which in turn change the rotating vibration characteristics of blades. As a result, the converged solution satisfies simultaneously the overall vehicle force and moment equilibrium equations.

Finite-Element Method in Time

From Hamilton's principle in weak form, the following virtual energy expression is obtained:

$$\int_{\psi_I}^{\psi_F} \delta q^T (M\ddot{q} + C\dot{q} + Kq - F)\, d\psi = 0 \tag{1}$$

where the associated matrices, i.e., the global mass M, damping C, stiffness K, and force vector F in the space domain, contain periodic terms. (All of the nonlinear terms are put in the force vector for convenience.) Integrating this equation by parts and rearranging gives the following reduced form:

$$\int_{\psi_I}^{\psi_F} \delta Y^T Q\, d\psi = \delta Y^T B \tag{2}$$

where

$$Y = \begin{Bmatrix} q \\ \dot{q} \end{Bmatrix}$$

$$Q = \begin{Bmatrix} F - C\dot{q} - Kq \\ M\dot{q} \end{Bmatrix}$$

$$B = \begin{Bmatrix} M\dot{q} \\ 0 \end{Bmatrix}_{\psi_I}^{\psi_F}$$

and ψ_I and ψ_F represent the initial and final states of time and B is a boundary term. For the periodic response solution, choosing $\psi_F = \psi_I + T$, where T is the time period of one rotor revolution (i.e., 2π), would result in dropping out the right-hand side of Eq. (2).

$$\int_{\psi_I}^{\psi_F} \delta Y^T Q\, d\psi = 0 \tag{3}$$

Using a first-order Taylor series expansion, the load vector Q can be linearized about the steady-state vector Y, such as

$$Q(Y + \Delta Y) = Q(Y) + \frac{\partial Q}{\partial Y} \Delta Y \tag{4}$$

Therefore, the linearized form of Eq. (3) is

$$\int_{\psi_I}^{\psi_F} \delta Y^T \{Q + K_t \Delta Y\}\, d\psi = 0 \tag{5}$$

where the local tangent matrix K_t is given as

$$K_t = \frac{\partial Q}{\partial Y} = \begin{bmatrix} \dfrac{\partial F}{\partial q} - K & \dfrac{\partial F}{\partial \dot{q}} - C \\ 0 & M \end{bmatrix}$$

For the analysis, one cycle of time is discretized into a number of time elements. Each time element is represented by a Lagrange polynomial along the azimuth. For N_e time ele-

ments, Eq. (5) can be written in a discretized form as

$$\sum_{i=1}^{N_e} \int_{\psi_i}^{\psi_{i+1}} \delta Y^T \{Q + K_t \Delta Y\} \, d\psi = 0 \tag{6}$$

where the ψ_i and ψ_{i+1} represent lower and upper time limits for the ith time element.

To reduce computation time, the global nodal displacement q in the space domain can be transformed to the normal coordinate p, using the normal mode Φ obtained from the eigenanalysis, such as

$$q = \Phi p \tag{7}$$

Therefore, the state vector Y can be expressed in terms of the normal coordinates X, as follows:

$$Y = \begin{Bmatrix} q \\ \dot{q} \end{Bmatrix} = \Psi X \tag{8}$$

where the modal transformation matrix Ψ and normal coordinates X are defined as

$$\Psi = \begin{bmatrix} \Phi & 0 \\ 0 & \Phi \end{bmatrix}$$

$$X = \begin{Bmatrix} p \\ \dot{p} \end{Bmatrix} \tag{9}$$

The displacement distribution of normal coordinates X is expressed in terms of the nodal normal coordinates X_i for the corresponding time element.

$$X = \begin{Bmatrix} p \\ \dot{p} \end{Bmatrix} = NX_i \tag{10}$$

The matrix for the elemental shape function of a time element N is given as

$$N = \begin{Bmatrix} N_T \\ \dot{N}_T \end{Bmatrix} = \begin{bmatrix} N_1 I, \ldots, N_{k+1} I \\ \dot{N}_1 I, \ldots, \dot{N}_{k+1} I \end{bmatrix} \tag{11}$$

where I is an identity matrix having the size of m, the number of normal modes, and the subscript k represents the order of the shape function along the azimuth. Thus, the size of the matrix N will be $2m \times m(k+1)$. For time variation, the interpolating polynomial for the shape function is taken from the Lagrange polynomial family. Rewriting the steady-state vector Y in terms of the nodal normal coordinates X_i using Eqs. (8-10), one would obtain the following expression:

$$Y = \begin{Bmatrix} q \\ \dot{q} \end{Bmatrix} = \Psi N X_i \tag{12}$$

By substituting this into Eq. (6), the finite-element equations are expressed as

$$\sum_{i=1}^{Ne} \int_{\psi_i}^{\psi_{i+1}} \delta X_i^T \{N^T \Psi^T Q + (N^T \Psi^T K_t \Psi N) \Delta X_i\} \, d\psi = 0 \tag{13}$$

The periodic boundary conditions are enforced for rotor steady response as

$$X(\psi_I = 0) = X(\psi_F = T) \tag{14}$$

Assembling the elemental finite-element equations, one obtains

$$\delta X_G^T (Q^G + K_t^G \Delta X_G) = 0 \tag{15}$$

where the global load vector and tangential stiffness matrix are

$$X_G = \sum_{i=1}^{N_e} X_i$$

$$Q^G = \sum_{i=1}^{N_e} \int_{\psi_i}^{\psi_{i+1}} N^T \Psi^T Q \, d\psi$$

$$K_t^G = \sum_{i=1}^{N_e} \int_{\psi_i}^{\psi_{i+1}} N^T \Psi^T K_t \Psi N \, d\psi \tag{16}$$

The ΔX_G is the incremental global vector of the normal coordinates. To calculate ΔX_G, a standard linear equation solver can be employed. The steady-state vector X_G is calculated iteratively using

$$X_G^{(n)} = X_G^{(n-1)} + \Delta X_G^{(n)} \tag{17}$$

where n is the step of iteration. For a converged solution, $\Delta X_G^{(n)}$ becomes nearly zero.

Design Sensitivity Analysis

In the present study, the sensitivity derivatives of blade response and hub loads, with respect to the design variables, are calculated using a direct analytical approach. Let us consider a general function F, which depends on the design variable D and blade response Y.

$$F = F[D, Y(D)] \tag{18}$$

The sensitivity derivatives of this function are calculated using a chain rule differentiation, as

$$\frac{dF}{dD_j} = \frac{\partial F}{\partial D_j} + \frac{\partial F}{\partial Y} \frac{\partial Y}{\partial D_j}, \qquad j = 1, \ldots, n \tag{19}$$

The sensitivity derivatives dF/dD_j, also called *directional derivatives*, are expressed in terms of the sensitivity derivatives of blade response, $\partial Y/\partial D_j$.

The finite-difference approach is frequently used to calculate the sensitivity derivatives. This approach is easy to implement, but costly because of heavy computation time. Also, a proper step size is sometimes difficult to determine. A direct analytical approach is very involved in formulation, but reduces the computation time substantially.

Steady Response Sensitivity Analysis

The formulation of the sensitivity derivatives of the blade response is developed as an integral part of the basic steady response analysis. For the derivatives of the blade steady response, the virtual energy expression [Eq. (3)] can be differentiated with respect to the design variables D_j.

$$\int_{\psi_I}^{\psi_F} \delta Y^T \frac{dQ}{dD_j} \, d\psi = 0, \qquad j = 1, \ldots, n \tag{20}$$

Using chain rule differentiation, the derivatives of load vector can be written as

$$\frac{dQ}{dD_j} = \frac{\partial Q}{\partial D_j} + \frac{\partial Q}{\partial Y} \frac{\partial Y}{\partial D_j}, \qquad j = 1, \ldots, n \tag{21}$$

Rewriting Eq. (20) gives

$$\int_{\psi_I}^{\psi_F} \delta Y^T \left\{ \frac{\partial Q}{\partial D_j} + K_t \frac{\partial Y}{\partial D_j} \right\} d\psi = 0, \qquad j = , \ldots, n \tag{22}$$

One would express the partial derivatives of the blade steady

response from Eq. (12) in terms of the derivatives of the nodal normal coordinates.

$$\frac{\partial Y}{\partial D_j} = \Psi N \frac{\partial X_i}{\partial D_j}, \qquad j = 1, \ldots, n \tag{23}$$

By substutiting this equation into Eq. (22), the derivatives of the virtual energy expression can be written for N_e time elements in the discretized form.

$$\sum_{i=1}^{N_e} \int_{\psi_i}^{\psi_{i+1}} \delta X_i^T N^T \Psi^T \left\{ \frac{\partial Q}{\partial D_j} + K_t \Psi N \frac{\partial X_i}{\partial D_j} \right\} d\psi = 0, \qquad j = 1, \ldots, n \tag{24}$$

One would then apply the following periodic boundary conditions for the derivatives of the steady response.

$$\frac{\partial X_i(\psi_I = 0)}{\partial D_j} = \frac{\partial X_i(\psi_F = T)}{\partial D_j}, \qquad j = 1, \ldots, n \tag{25}$$

Assembling the elemental finite-element equations over time elements results in the following form:

$$\delta X_G^T \left(\frac{\partial Q^G}{\partial D_j} + K_t^G \frac{\partial X_G}{\partial D_j} \right) = 0 \tag{26}$$

This gives

$$\frac{\partial X_G}{\partial D_j} = -(K_t^G)^{-1} \frac{\partial Q^G}{\partial D_j}, \qquad j = 1, \ldots, n \tag{27}$$

where

$$\frac{\partial Q^G}{\partial D_j} = \sum_{i=1}^{N_e} \int_{\psi_i}^{\psi_{i+1}} N^T \Psi^T \frac{\partial Q}{\partial D_j} d\psi$$

$$\frac{\partial Q}{\partial D_j} = \begin{bmatrix} \dfrac{\partial F}{\partial D_j} - \dfrac{\partial C}{\partial D_j}\dot{q} - \dfrac{\partial K}{\partial D_j} q \\ \dfrac{\partial M}{\partial D_j}\dot{q} \end{bmatrix} \tag{28}$$

It is noted that the partial derivatives of mass, damping and stiffness matrices, and force vector are analytically calculated using the virtual energy expression.

Hub Loads Sensitivity Analysis

Using a force summation method, the blade loads at the root are calculated by summing the aerodynamic and inertial loads along the blade. The hub loads are obtained by transforming these blade root loads into the hub-fixed nonrotating frame and then summing these for all blades.

$$F_H = \sum_{n=1}^{N_b} T_C^T F_R^{(n)}$$

$$M_H = \sum_{n=1}^{N_b} T_C^T M_R^{(n)} \tag{29}$$

where the subscripts R and H represent, respectively, the rotating (undeformed blade) frame and hub-fixed nonrotating frame. The matrix T_C is a transformation matrix from the underformed blade frame to the hub-fixed nonrotating frame, and is defined in Refs. 15 and 18.

The derivatives of hub loads with respect to the design variables are taken

$$\frac{dF_H}{dD_j} = \sum_{n=1}^{N_b} T_C^T \frac{dF_R^{(n)}}{dD_j}, \qquad j = 1, \ldots, n$$

$$\frac{dM_H}{dD_j} = \sum_{n=1}^{N_b} T_C^T \frac{dM_R^{(n)}}{dD_j} \tag{30}$$

The detailed expressions for blade root forces and moments are given in Ref. 15.

For a four-bladed rotor, the 4/rev harmonics of hub loads in the hub-fixed nonrotating frame are the primary source of vibration in the airframe. The other harmonics are either cancelled out or are of low significance to cause vibration. These harmonics are defined in terms of cosine and sine terms. As an example, the 4/rev vertical hub shear is given as

$$F_{zH}^{4P} = \sqrt{(F_{zH}^{4c})^2 + (F_{zH}^{4s})^2}$$

The derivatives of oscillatory hub loads are obtained by differentiating the harmonics of hub loads with respect to the design varibles. For a 4/rev vertical hub shear, the corresponding derivatives are expressed as

$$\frac{dF_{zH}^{4P}}{dD_j} = \frac{F_{zH}^{4c} \dfrac{dF_{zH}^{4c}}{dD_j} + F_{zH}^{4s} \dfrac{dF_{zH}^{4s}}{dD_j}}{F_{zH}^{4P}}, \qquad j = 1, \ldots, n \tag{31}$$

where

$$\frac{dF_{zH}^{4c}}{dD_j} = \frac{1}{\pi} \int_0^{2\pi} \frac{dF_{zH}(\psi)}{dD_j} \cos 4\psi \, d\psi$$

$$\frac{dF_{zH}^{4s}}{dD_j} = \frac{1}{\pi} \int_0^{2\pi} \frac{dF_{zH}(\psi)}{dD_j} \sin 4\psi \, d\psi \tag{32}$$

In the same manner, the derivatives of other harmonics can be obtained.

For inertial loads, one needs to calculate the steady acceleration. The straightforward approach is to differentiate the steady response with respect to time.

$$\ddot{q}(\psi) = \Phi \ddot{N}_T X_i \tag{33}$$

This approach is easy to implement, but the reduction of the order of the shape function due to differentiation may give a large numerical error for the steady acceleration. For example, if a cubic polynomial is used to represent the steady response along the azimuth, a linear polynomial results for the steady acceleration, and this would give a poor estimate for inertial forces. In order to predict the steady acceleration accurately, one needs either a larger number of time elements or a higher order polynomial distribution within each time element.

An alternative approach is to derive the steady acceleration directly from the equations of motion.

$$\ddot{q}(\psi) = M^{-1}[F - C\dot{q} - Kq] \tag{34}$$

This approach helps to reduce the numerical difficulties associated with simple differentiation of the shape functions for the steady acceleration. Although it would make the formulation more involved, it is an efficient approach for calculation of the steady acceleration.

The mass, damping, and stiffness matrices do not contain the nonlinear terms because they are put into the force vector for convenience. Hence, the directional derivatives of the mass, damping, and stiffness matrices are equivalent to the partial derivatives, and the derivatives of the steady acceleration would be expressed as

$$\frac{\partial \ddot{q}}{\partial D_j} = M^{-1} \left\{ \frac{\partial F}{\partial D_j} - \frac{\partial M}{\partial D_j}\ddot{q} - \frac{\partial C}{\partial D_j}\dot{q} - \frac{\partial K}{\partial D_j} q + \left(\frac{\partial F}{\partial q} - K \right) \frac{\partial q}{\partial D_j} + \left(\frac{\partial F}{\partial \dot{q}} - C \right) \frac{\partial \dot{q}}{\partial D_j} \right\} \tag{35}$$

The mass, damping, and stiffness matrices, and their partial derivatives, with respect to the design variables, are derived analytically from the virtual energy expression, and are available in Ref. 15.

Table 1 Baseline hingeless blade structural properties

$$EI_y/m_0\Omega^2R^4 = 0.01080$$
$$EI_z/m_0\Omega^2R^4 = 0.02680$$
$$GJ/m_0\Omega^2R^4 = 0.00615$$
$$k_A/R = 0.0290$$
$$k_{m1}/R = 0.0132$$
$$k_{m2}/R = 0.0247$$

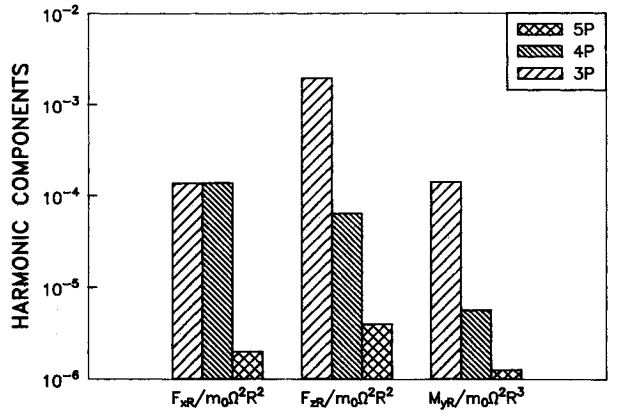

Fig. 1 Harmonics of blade root loads in rotating frame (F_{xR} = radial shear, F_{zR} = vertical shear, M_{yR} = flap moment).

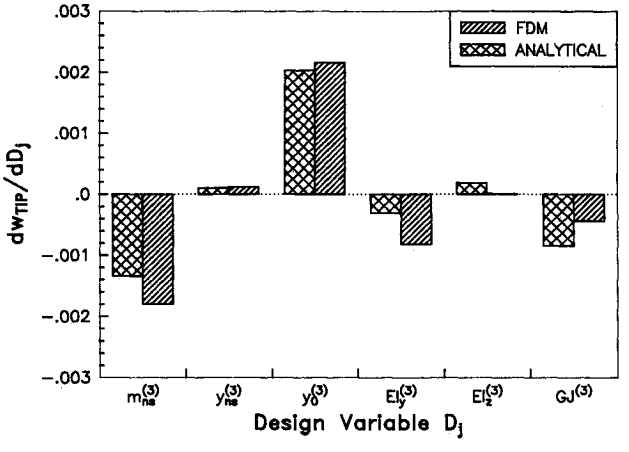

Fig. 2 Derivatives of steady flap response at tip with respect to design variables at midspan.

Results and Discussion

Numerical results are calculated for a four-bladed, soft-in-plane hingeless rotor with Lock number $\gamma = 5.5$, solidity ratio $\sigma = 0.07$, thrust level $c_W/\sigma = 0.07$, blade aspect ratio $c/R = 0.55$, zero precone and zero pretwist. The chordwise locations of blade center of gravity, aerodynamic center, and tensile axis from the elastic axis (e_g, e_d, and e_A), are assumed to be zero for the baseline configuration. The fuselage center of gravity lies on the shaft axis ($X_{CG} = Y_{CG} = 0$), and is located at a distance $0.2R$ below the rotor hub center. The fuselage drag coefficient in terms of flat plate area, i.e., $f/\pi R^2$ is taken as 0.01. The airfoil characteristics used are $c_\ell = 2\pi\alpha$, $c_d = 0.01$, and $c_m = 0.0$. For the baseline blade configuration, the structural properties of the blade are assumed uniform and given in Table 1. The first flap, lag, and torsional frequencies are 1.13, 0.70, and 4.47/rev, respectively. The numerical results are calculated for an advance ratio of 0.3.

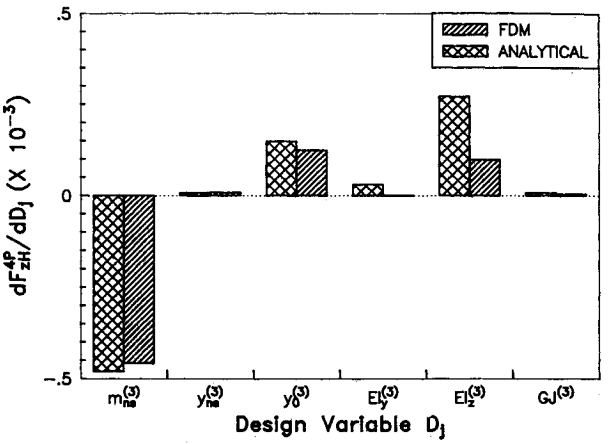

Fig. 3 Derivatives of 4/rev vertical hub shear with respect to design variables at midspan (4-bladed rotor).

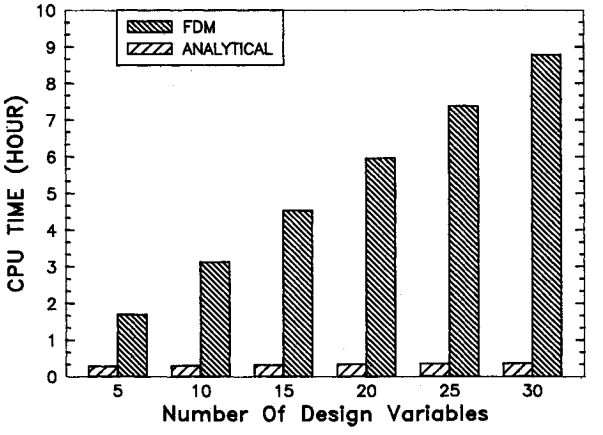

Fig. 4 CPU time required on UNISYS 1100/90 for calculation of derivatives of blade response and hub loads.

For the analysis, the blade is discretized into five beam elements of equal length, and each beam element consists of 15 nodal degrees of freedom. To reduce the computation time, 8 coupled rotating natural modes (2 flap, 2 lag, 2 torsion, and 2 axial modes) are used. For the periodic steady response of the rotor, one cycle of time is discretized into six time elements and each time element is described by a quartic Lagrange polynomial distribution along the azimuth.

The rotor transmits the harmonic components from the rotating frame to the airframe (nonrotating frame) in the form of hub loads. For a four-bladed rotor, the transmitted hub loads consist primarily of 4/rev hamonics in the nonrotating frame. The 4/rev longitudinal and lateral hub shears in the hub-fixed nonrotating frame originates from the 3/rev and 5/rev harmonics of the inplane (radial and chordwise) root shears in the rotating frame, and the 4/rev harmonics of the inplane root shears get cancelled through summation over all blades. The 4/rev vertical shear force originates from the 4/rev vertical root shear over all blades. The 3/rev vertical root shear, though a very dominating harmonic component in the rotating frame, gets cancelled at the hub level. For vibration reductions in the airframe, one can, therefore, overlook the 4/rev inplane root shears and 3/rev vertical root shear. The 4/rev rolling and pitching hub moments in the hub-fixed nonrotating frame originate from 3/rev and 5/rev harmonics of the flapwise blade root moments in the rotating frame, and the 4/rev flapwise root moments get cancelled through summation over all blades. Therefore, one can ignore the 4/rev hamonic of the flapwise root moments. The 4/rev yawing hub

moment originates from the 4/rev lagwise root moments in the rotating frame. The 3/rev and 5/rev harmonics get cancelled through summation over all blades. Therefore, for vibration in the airframe, the 3/rev harmonic is important for the in-plane shears (radial and chordwise) and flapwise moment, and the 4/rev harmonic is important for the vertical root shear and lagwise moment. It may be noted that the 5/rev harmonic of the blade root forces and moments is quite negligible as compared with the 3/rev harmonic. As an example, the higher harmonic components of radial and vertical blade root shears and flapwise blade root moment are shown in Fig. 1.

Design sensitivity analysis involves calculation of the sensitivity derivatives of the steady response and hub loads. To calculate the derivatives, a direct analytical approach is used, and the numerical results are compared with the finite-difference approach. For the finite-difference approach, a central difference scheme with 3% perturbations on either side of the baseline values is used. Structural design parameters are nonstructural mass m_{ns}, chordwise offset of nonstructural mass from the elastic axis y_{ns}, blade center of gravity offset from the elastic axis y_o, blade flap bending stiffness EI_y, lag bending stiffness EI_z, and torsional stiffness GJ. Furthermore, these design parameters have spanwise variations; therefore, a total of 30 design variables for 5 beam elements are involved in the analysis.

Figure 2 compares the sensitivity derivatives of the steady flap tip response at $\psi = 0$ deg, with respect to the design variables at the midspan location (third element). The numerical results obtained by finite-difference and direct analytical approaches show identical trends. Figure 3 compares the sensitivity derivatives of the 4/rev vertical hub shear in the nonrotating frame with respect to the design variables at the midspan location. Again, the numerical results by finite-difference and direct analytical approaches show identical trends.

Figure 4 shows the CPU time required in UNISYS-1100/90 for calculation of the sensitivity derivatives of the blade steady response and oscillatory hub loads, using finite-difference and analytical approaches. For the finite-difference approach, the CPU time is estimated based on the number of function evaluations. The CPU time required for the derivatives increases linearly with respect to the number of design variables when the finite-difference approach is used, whereas it is only slightly increased by the use of the direct analytical approach. For 30 design variables, the CPU time with the finite-difference approach is 530 min, whereas it is 22 min with the analytical approach. There is a substantial reduction in computation time with the direct analytical approach (96% CPU time reduction for 30 design variables).

Figure 5 shows the effect of nonstructural mass distribution on the oscillatory hub force and moment in the rotating frame. For this, an additional concentrated mass of 5% of the baseline blade mass is placed at different spanwise and chordwise locations. It is quite clear that the best location to add nonstructural mass for vibration reductions is at the outboard station, for example, around the 70% spanwise location (second element) for the vertical shear and flapwise hub moment. With a 5% extra weight at this spanwise location, reductions of 15% for the vertical hub shear and 17% for the hub

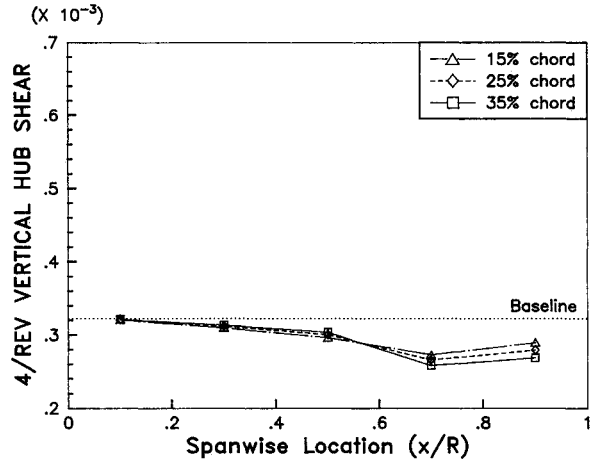

Fig. 5a Effect of nonstructural mass (5% of baseline blade mass) placement on 4P vertical hub shear.

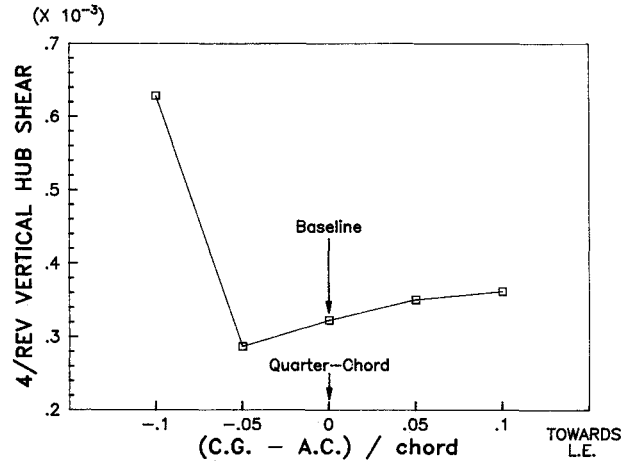

Fig. 6a Effect of blade center of gravity offset (uniform) on 4P vertical hub shear.

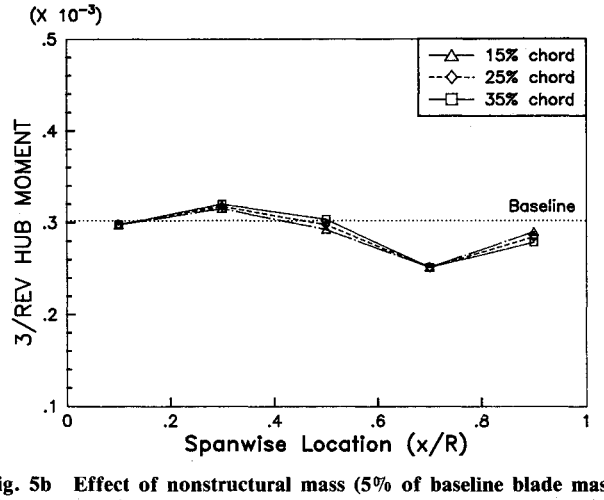

Fig. 5b Effect of nonstructural mass (5% of baseline blade mass) placement on 3P hub moment in rotating frame.

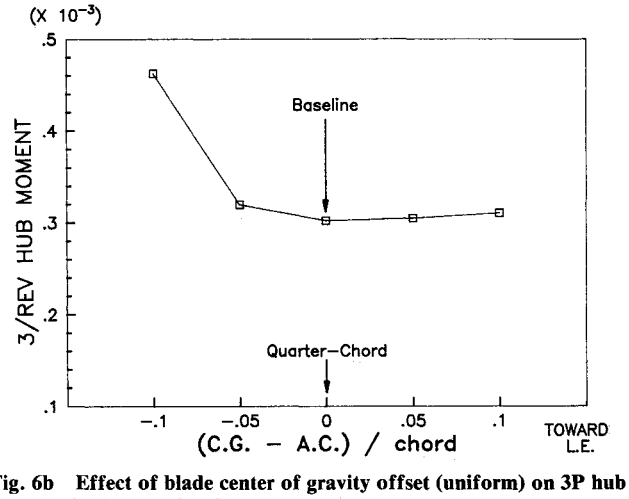

Fig. 6b Effect of blade center of gravity offset (uniform) on 3P hub moment in the rotating frame.

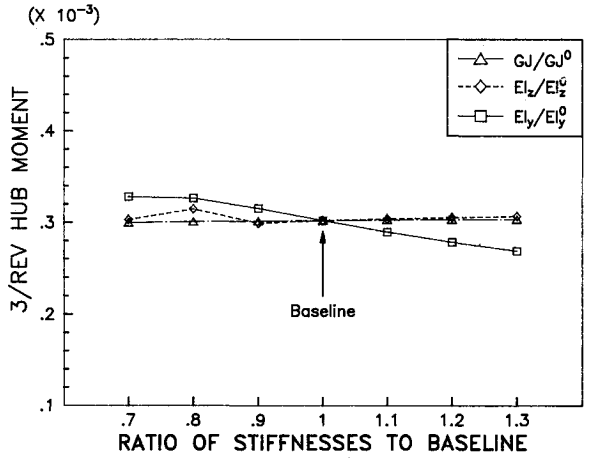

Fig. 7a Effect of blade bending stiffness on second lag mode.

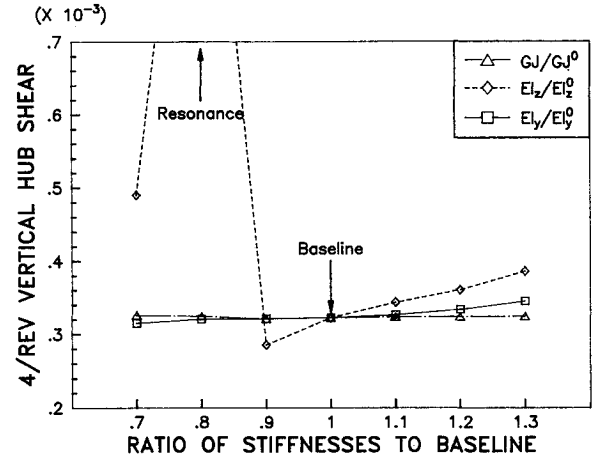

Fig. 7b Effect of blade bending stiffnesses on 4P vertical hub shear.

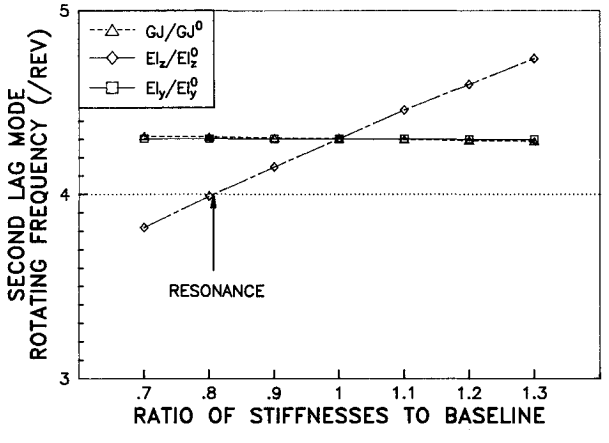

Fig. 7c Effect of blade bending sitffnesses on 3P hub moment in the rotating frame.

moment are achieved. For these calculations, the aerodynamic center and elastic axis are assumed to be at the quarter-chord position. A concentrated mass increases the blade inertia and also increases spring stiffness due to the centrifugal stiffening. Toward the blade tip, the centrifugal stiffening is dominating, and with a concentrated mass near the blade tip the oscillatory hub loads are lower than the baseline values. When a concentrated mass is near the blade root, centrifugal stiffening effects become smaller, and the oscillatory hub loads are generally higher. Furthermore, the addition of the nonstructural mass changes the blade center of gravity as well as the blade mass. The chordwise offset of blade c.g. would induce coupling of torsional and flap responses. Lag response is also coupled with these responese, due to the Coriolis effect. By suitable placement of nonstructural masses, one can get favorable effects from these couplings. Around the 70% spanwise location, the addition of a nonstructural mass of 5% blade mass at the 35% chord position (aft) can reduce the 4/rev vertical shear by 6% from the value obtained by placing this mass at 15% chord position (forward). The forward location of nonstructural mass is generally favorable for vibration reduction, except near the blade tip where the aft location is more favorable. These results show that the location of nonstructural mass (chordwise and spanwise) has a powerful effect on the oscillatory hub loads.

Figure 6 shows the influence on the oscillatory hub force and moment in the rotating frame due to the uniform change of the blade center of gravity offset along the blade span. The elastic axis is assumed to coincide with the aerodynamic center (quarter-chord position). The chordwise offset of blade c.g. is shifted forward (positive) or aft (negative) from the elastic axis uniformly along the blade span. The blade mass is held fixed as the baseline value. The blade c.g. offset induces coupling of torsional and flap responses. An aft position (say, 35% chord) of the blade c.g. may result in the torsion mode instability, where the hub force and moment sharply increase. The 4/rev vertical hub shear increases by a forward shift, and decreases by an aft shift of the blade c.g. from the elastic axis. However, a little further shift toward the trailing edge (more than 30% chord) would result in a sharp increase of the vertical hub shear, due to the instability of the torsion mode. The 3/rev hub moment in the rotating frame is comparatively less sensitive to blade c.g. offset, except for the sharp increase near the 35% chord, due to the instability.

The change of blade bending stiffnesses would change the natural frequencies of the blade. For example, a 20% uniform increase in flap bending stiffness (EI_y) along the blade span would raise its flap frequency from 1.13 to 1.14/rev, a 20% increase in lag bending stiffness (EI_z) would raise its lag frequency from 0.70 to 0.75/rev, and a 20% increase in torsional stiffness (GJ) would change the torsional frequency from 4.47 to 4.88/rev. The smallest change in the rotating frequency due to the stiffness change occurs in the flap mode, because its stiffneess is derived less from elasticity and more from centrifugal force.

Figure 7 shows the sensitivity of the oscillatory hub loads in the rotating frame with respect to blade bending stiffnesses, i.e., flap bending stiffness (EI_y), lag bending stiffness (EI_z), and torsional stiffness (GJ). The superscript "0" denotes the baseline value. The second lag mode rotating frequency for the baseline value is 4.3/rev. With reduced lag bending stiffness, it comes closer to 4/rev and a resonance condition is possible (see Fig. 7a). For the 4/rev vertical hub shear, the largest influence is due to the lag bending stiffness. A slight reduction of the lag bending stiffness from the baseline value reduces the vertical hub shear, but a further reduction (less than 90% of the baseline value) aggravates the vertical hub shear, due to the resonance of the second lag mode. The softening of the flap bending stiffness somewhat reduces the vertical hub shear, whereas the stiffening increases it, and the influence of the torsional stiffness on the vertical hub shear is quite small. For the 3/rev hub moment, the largest influence is due to the flap bending stiffness. One would expect that the larger the flap bending stiffness, the larger bending moments are transmitted to the hub. But here the opposite is happening. The softening of the flap bending stiffness increases the hub moment, and the stiffening reduces the moment. The variation of the lag bending stiffness has a small effect on the hub moment. Again, the variation of the torsional stiffness has a negligible influence on the hub moment. The hub moment does not show any influence, due to the resonance at 4/rev, because it originates from 3/rev and 5/rev blade root loads.

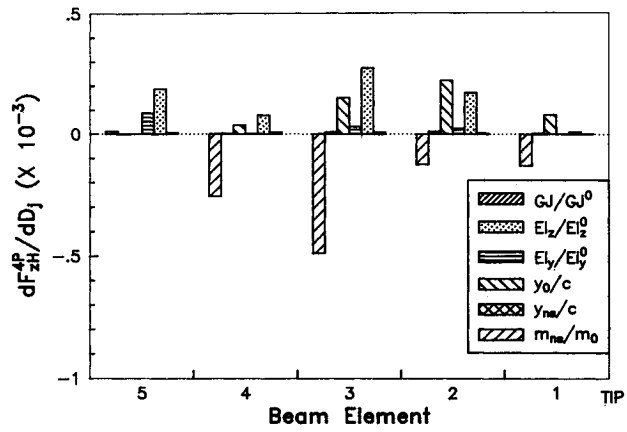

Fig. 8 Derivatives of 4/rev vertical hub shear with respect to design variables.

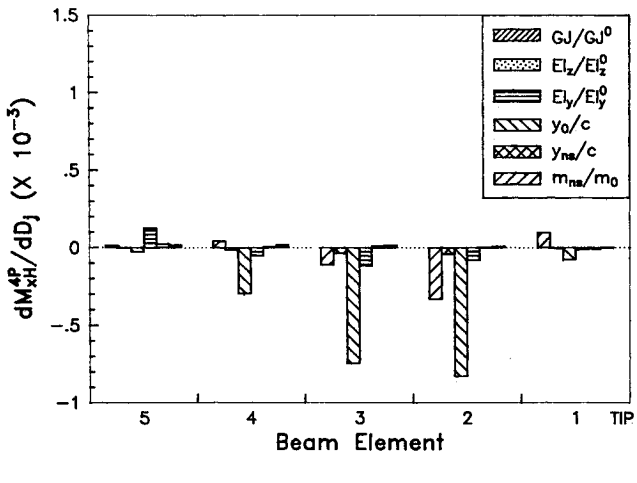

Fig. 9 Derivatives of 4/rev rolling hub moment (fixed frame) with respect to design variables.

In Figs. 8 and 9, the sensitivity derivatives of the 4/rev hub forces and moments in the hub-fixed nonrotating frame at different spanwise locations are shown. These derivatives are calculated at the baseline configuration using the direct analytical approach and with an additional nonstructural mass of 5% blade mass. By examining the magnitude of the derivatives, the sensitivity with respect to each design variable can be studied. The 4/rev vertical hub shear is quite sensitive to nonstructural mass, blade c.g. offset, and lag bending stiffness. It confirms earlier observations made in Figs. 5a, 6a, and 7b. For the 4/rev inplane hub moment (rolling), the largest influence is due to the nonstructural mass and blade c.g. offset; again, similar trends are observed in Figs. 5b and 6b.

Conclusions

Based on the preceding results, the following conclusions are made:

1) A direct analytical approach is used successfully to calculate the sensitivity derivatives of blade steady response and oscillatory hub loads, and shows a substantial reduction of CPU time compared with the finite-difference approaches. A 96% reduction of CPU time is achieved by using a direct analytical approach for calculation of the senstivity derivatives of blade response and oscillatory hub loads with respect to 30 design variables.

2) The 4/rev vertical hub shear is sensitive to nonstructural mass, blade c.g. offset, and lag bending stiffness. Adding nonstructural mass, an aft shift of blade c.g. for outboard elements, or softening of lag bending stiffness reduces the 4/rev vertical shear considerably.

3) The 4/rev inplane hub moment (rolling) is sensitive to nonstructural mass and blade c.g. offset. Adding nonstructural mass at outboard elements or a forward shift of blade c.g. for outboard elements reduces the 4/rev hub moment considerably.

Recently, as described in Ref. 19, these analytically derived response sensitivity derivatives were implemented successfully in the optimization process to minimize oscillatory hub loads for a typical hingeless rotor in forward flight. The optimization process was quite robust, and there was a substantial reduction of computation time (about 80%) to achieve the optimum solution, compared with the frequently used finite-difference approach.

Acknowledgment

This work is supported by NASA Langley Research Center under NASA Grant NAG-1-739; technical monitor Joanne Walsh.

References

[1]Ashley, H., "On Making Things the Best—Aeronautical Uses of Optimization," *Journal of Aircraft*, Vol. 19, Jan. 1982, pp. 5-28.

[2]Blackwell, R. H., "Blade Design for Reduced Helicopter Vibration," *Journal of the American Helicopter Society*, Vol. 28, No. 3, July 1983, pp. 33-41.

[3]Taylor, R. B., "Helicopter Vibration Reduction by Rotor Blade Modal Shaping," *Proceedings of the 38th American Helicopter Society Annual Forum*, May 1982.

[4]Friedmann, P. P. and Shanthakumaran, P., "Optimum Design of Rotor Blades for Vibration Reduction in Forward Flight," *Journal of the American Helicopter Society*, Vol. 29, No. 4, Oct. 1984, pp. 70-80.

[5]Miura, H. and Schmit, L. A., "NEWSUMT—A Fortran Program for Inequality Constrained Function Minimization," User's Guide, NASA CR-159070, 1979.

[6]Peters, D. A., Rossow, M. P., Korn, A., and Ko, T., "Design of Helicopter Rotor Blades for Optimum Dynamic Characteristics," *Comp. & Math. with Applications*, Vol. 12A, Jan. 1986, pp. 85-109.

[7]Vanderplaats, G. N., "CONMIN—A Fortran Program for Constrained Function Minimization," User's Manual, NASA TMX-62282, 1973.

[8]Davis, M. W. and Weller, W. H., "Application of Design Optimization Techniques to Rotor Dynamics Problems," *Proceedings of the 42nd American Helicopter Society Annual Forum*, Washington, DC, June 1986, pp. 27-44.

[9]Vanderplaats, G. N., Sugimoto, H., and Sprague, C. M., "ADS-1: A New General Purpose Optimization Program," *AIAA Journal*, Vol. 22, Oct. 1984, pp. 1458-1459.

[10]Yen, J. G., "Coupled Aeroelastic Hub Loads Reduction," AHS/NAI International Seminar, Nanjing, China, Nov. 1985.

[11]Adelmann, H. M. and Haftka, R. T., "Sensitivity Analysis of Discrete Structural Systems," *AIAA Journal*, Vol. 24, May 1986, pp. 823-832.

[12]Johnson, W., "Recent Development in the Dynamics of Advanced Rotor Systems," NASA TM-86669, March 1985.

[13]Friedmann, P. P., "Formulation and Solution of Rotary Wings Aeroelastic Stability and Response Problems," *Vertica*, Vol. 7, No. 2 April 1983, pp. 101-141.

[14]Panda, B. and Chopra, I., "Dynamics of Composite Rotor Blades in Forward Flight," *Vertica*, No. 1/2, Jan. 1987, pp. 187-209.

[15]Lim, J. W., "Aeroelastic Optimization of a Helicopter," Ph.D. Dissertation, Dept. of Aerospace Engineering, Univ. of Maryland, College Park, MD, May 1988.

[16]Johnson, W., *Helicopter Theory*, Princeton Univ. Press, Princeton, NJ, 1980.

[17]Lim, J. W. and Chopra I., "Stability Sensitivity Analysis for Aeroelastic Optimization of a Helicopter Rotor," *Proceedings of the AIAA/ASME/ASCE/AHS 29th Structures, Structural Dynamics and Materials Conference*, AIAA, Washington, DC, April 1988.

[18]Bir, G. S. and Chopra, I., "Gust Response of Hingeless Rotors," *Journal of the American Helicopter Society*, Vol. 31, No. 2, April 1986, pp. 33-46.

[19]Lim, J. W. and Chopra, I., "Aeroelastic Optimization of a Helicopter Rotor," *Journal of the American Helicopter Society*, Vol. 34, No. 1, Jan. 1989, pp. 52-62.